Electronic Supplementary Material (ESI) for Journal of Materials Chemistry C.

Surface Modification with Fluorinated N-Heterocyclic Carbene on Au: Effect on Contact Resistance in Organic Field Effect Transistors

Zhifang Wang[‡a,b], Mowpriya Das[‡c], Christian Gutheil[c], Helena Osthues[d], Felix Strieth-Kalthoff[e], Alexander Timmer[e], Nikos L. Doltsinis[d] , Wenchong Wang*[b], Lifeng Chi*[a,b] and Frank Glorius*[c]*

a. Institute of Functional Nano & Soft Materials (FUNSOM), Jiangsu Key Laboratory for Carbon-Based Functional Materials & Devices, Soochow University, 199 Ren'ai Road, Suzhou, 215123, Jiangsu, P.R. China
b. Physikalisches Institut and Center for Nanotechnology (CeNTech), Westfälische Wilhelms-Universität Münster, Wilhelm-Klemm-Straße 10, 48149 Münster, Germany.
c. Organisch-Chemisches Institut, Westfälische Wilhelms-Universität Münster, Corrensstraße 36, 48149 Münster, Germany.
d. Institute for Solid State Theory and Center for Multiscale Theory and Computation, Westfälische Wilhelms-Universität Münster, Wilhelm-Klemm-Straße 10, 48149 Münster, Germany.
e. NanoAnalytics GmbH, Heisenbergstraße 40, 48149 Münster, Germany.

1. Materials and instruments

2,7-dioctyl[1]benzothieno[3,2-b][1]benzothiophene (C8-BTBT, ⩾99% HPLC), 6,13-bis((triisopropylsilyl)ethynyl)pentacene (TIPS-Pen, ⩾99% HPLC) and Toluene (anhydrous, 99.8%) were purchased from Sigma-Aldrich Chemie GmbH, which were used without further purification. The silicon wafers with 300 nm SiO_2 layer (C_i=10 nF

cm^{-2}) were selected as substrates, purchased from Si-Mat company, and cut into 1.5 cm×2 cm for the next use. The metal materials of chromium and gold were purchased from the ChemPur company with a purity of 99.9%. Commercially available chemicals were obtained from Acros Organics, Sigma-Aldrich, Alfa Aesar, ABCR, TCI Europe, Combi-Blocks, Johnson-Matthey and Heraeus and used as received unless otherwise stated.

The Au electrodes were deposited on the SiO_2 surface by thermal evaporation through a shadow mask at 0.3 nm/s rate using the evaporation system Edwards E306 with tungsten wire as heating source under a vacuum of 10^{-4} Pa.

^{1}Hand^{13}C-NMR spectra were recorded at room temperature on a Bruker AV 300 or AV 400 and Agilent 600 (DD2). Chemical shifts (δ) were given in ppm. The residual solvent signals were used as references and the chemical shifts converted to the TMS scale (CDCl3: δH = 7.26 ppm, δC = 77.16 ppm; DMSO-d6: δH = 2.50 ppm, δC = 39.52 ppm). Coupling constants (J) are quoted in Hz.

XPS measurements were performed using a K-Alpha + XPS instrument (ThermoFisher Scientific, UK) quipped with Al Kα microfocused monochromatized excitation source with photon energy 1486.6 eV operating at a base pressure of (5.0×10^{-9}) mbar. All samples were analyzed in Constant Analyzer Energy mode using a 400 μm spot size with a pass energy of 200 eV for survey and 20 eV for high-energy resolution spectra. The data acquisition was performed using the Thermo Avantage software and the processing was performed via CasaXPS. The angle of incidence was 60° with respect to the sample surface normal and an electron take off angle of 90º relative to the sample surface was set. Surface charge neutralization was performed utilizing the K-Alpha + dual compensation charge system which employs electrons and low-energy argon ions to prevent any localized charge build-up.

Atomic force microscopy (AFM) measurements were performed in air by a Multimode Nanoscope IIIa instrument (Digital Instrument) in tapping mode with n^{+}-silicon tip. (Type: PPP-NCH-W, resistivity: 0.01-0.02 Ωcm, Thickness: 4±1 μm /

Length: 125±10 μm / Width: 30±7.5 μm, Resonance Frequency: 204-497 kHz, Force Constant: 10-130 N/m, Tip height: 10-15 μm). Zeiss Axioplan microscope was performed to characterize the overall of the transistors.

Transfer and output characteristics were measured in the atmosphere with a Keithley 4200 SCS semiconductor parameter analyzer and a Micromanipulator 6150 probe station from Micromanipulator Co., Inc. using 7B Tungsten Probe Tips.

2. Synthetic procedure and characterization of fluorinated imidazolium salt

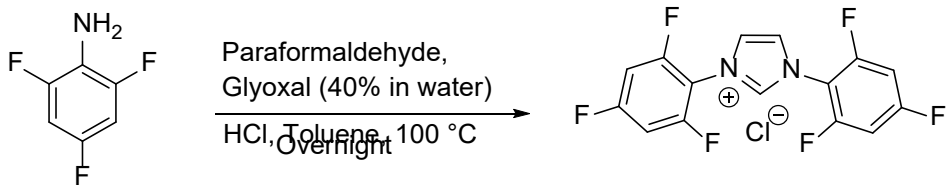

Scheme S1. Synthetic route for fluorinated imidazolium salt (F-NHC precursor).

The starting material imidazolium salt (NHC precursor) was synthesized following the synthetic route in the reference.[1] To a stirred solution of 2,4,6-trifluroaniline in dry toluene was added paraformaldehyde and then resulting mixture was heated to 100 °C. After getting dissolved all the solids, the resulting solution was cooled down to 40 °C and glyoxal solution in water (40 % solution in water) was added slowly. The solution was stirred for additional 5 minutes at the same temperature, and HCl was added dropwise. The mixture was heated to 100 °C for 12 hours. After cooling to room temperature, the solvent was removed by vacuum rotary evaporator. After adding diethyl ether, the solid was collected via filtration and washing with diethyl ether several times give the desired imidazolium salt as a pure white solid.

^{1}H NMR (400 MHz, DMSO-*d*$_6$) δ 10.36 (s, 1H), 8.51 (s, 2H), 7.78 (m, 4H).

^{19}F NMR (377 MHz, DMSO-*d*$_6$) δ -117.19 (br s, 4F, ArF), -99.80 (Br s, 2F, ArF).

IR: ν_{max}/cm^{-1} 3025br, 1616s, 1561s, 1495s, 1457s, 1258s, 1189s, 1133s, 1075s, 996s, 897br.

HRMS (ESI): calcd. for $C_{15}H_7F_6N_2$ $[M\text{-}Cl]^+$ 329.0507, found 329.0503.

3. Functionalization of Au-electrode with fluorinated N-heterocyclic carbene

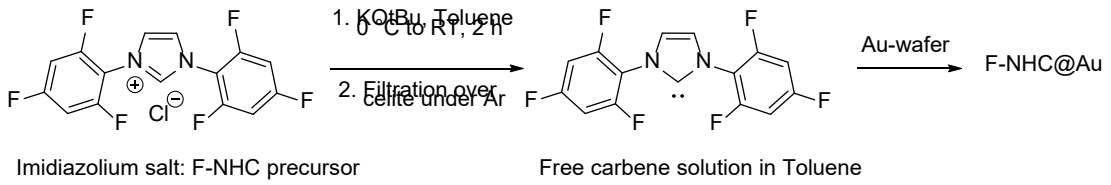

Scheme S2. Procedure for synthesizing of free carbene and modifying the gold surface with carbene solution.

Electrode modification with free carbene solution was performed according to a modified literature procedure.[2] All glassware and celite were stored in a 120 °C oven for overnight and flame-dried three times in vacuum before use. Filtration of free carbene solution over celite was performed using Schlenk-technique under inert atmosphere.

Free carbene solution was prepared by following modified literature procedure.[3,4] The fluorinated imidazolium salt (36.5 mg, 0.1 mmol, 1.0 equiv.) was taken in a dry 10 mL Schlenk red-cap flask and then potassium tert-butoxide (11.2 mg, 0.1 mmol, 1.0 equiv.) was added from the glove box. 2 mL of dry toluene was added to the flask under Ar atmosphere. The reaction mixture was allowed to stir at 0 °C for one hour and at room temperature for another one hour. After that, the solution of the resulting free carbene (F-NHC) in toluene was then transferred by syringe to the oven and flame-dried filtration apparatus containing celite under inert atmosphere. It was diluted to a 5 mM solution by addition of another 18 mL of dry toluene. An oven-dried and argon-purged flat-bottom 50 mL Schlenk flask fitted with a platform, under which a stir bar was placed and above which the gold electrode was secured. Under Ar atmosphere, 20 mL of the freshly prepared 5 mM of F-NHC solution in toluene was transferred to the 50 mL Schlenk flask containing the gold electrode. The solution was allowed to stir at 300 rpm in the presence of the electrodes overnight. After overnight stirring, the gold electrode wafers were washed with water and acetone under air and dried with stream of argon.

4. X-ray photoelectron spectroscopy (XPS) measurements

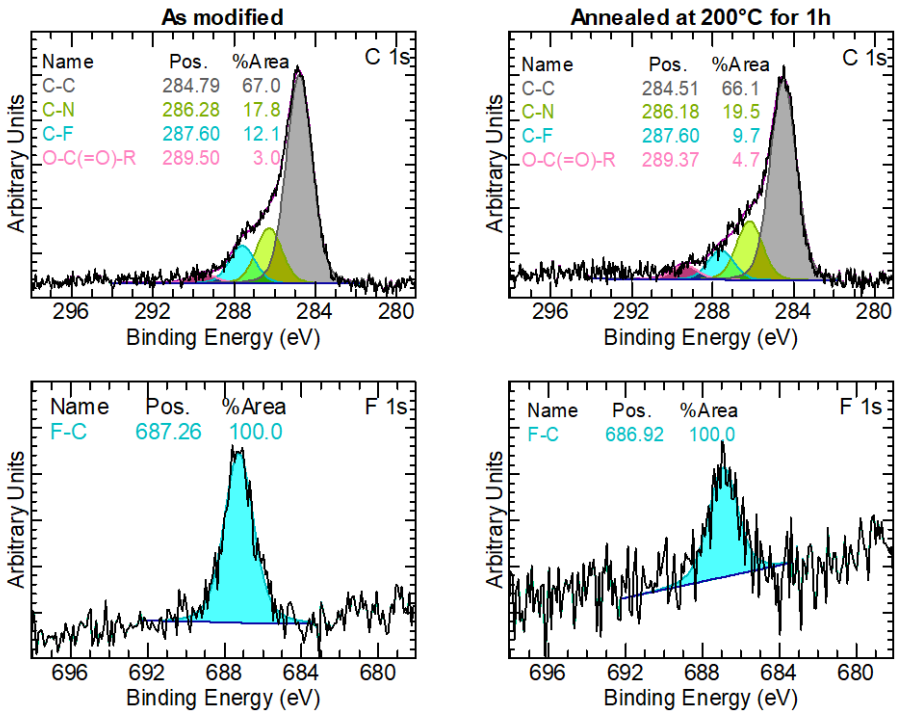

Figure S1. XPS spectra for the elements C(1s) and F(1s) of F-NHC on the gold surface before and after annealing.

5. Characterization of transistors

1) Morphology characterization

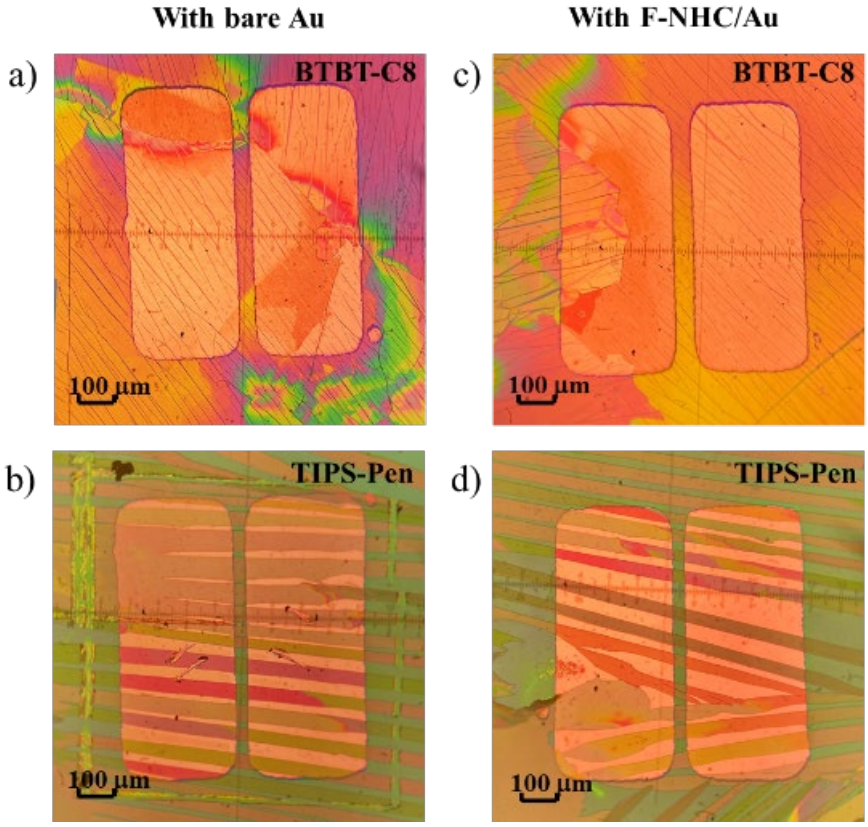

Figure S2. Optical microscope images of C8-BTBT and TIPS-Pen devices **a,b)** without modification, **c,d)** with F-NHC modification.

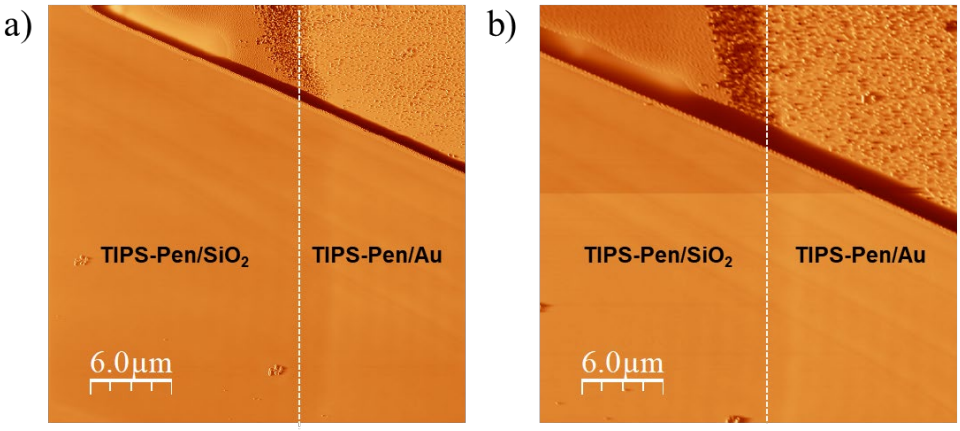

Figure S3. AFM phase images at the interface for TIPS-Pen transistor **a)** without modification **b)** with F-NHC modification.

2） Extraction of contact resistance

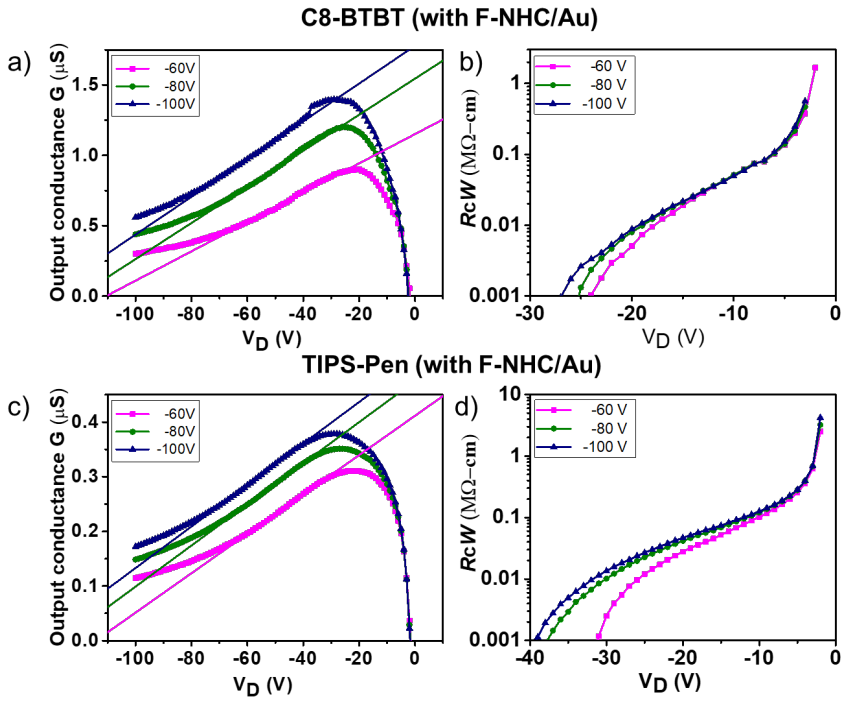

Figure S4. a,b) The graphs of output conductance G and R_cW as a function of source-drain voltage V_D at different gate-source voltages (-60 V, -80 V and -100V) for C8-BTBT transistor with F-NHC modified electrodes. **c,d)** Corresponding graphs for TIPS-Pen transistor with F-NHC modified electrodes.

The output conductance G as a function of V_D for the devices with F-NHC modified Au were measured using the G-function method, as shown in Figure S4a and c. G increases first and then decreases as V_D increases, which is consistent with a non-Ohmic contact characteristic reported in the literature.[5] Based on this, the curves of R_cW vs V_D can be determined through the Equation 2 (Figure S4b and d). W represents the channel width of 1000 μm.

The G-function expresses the output conductance G (unit in S or Ω^{-1}) versus V_D, which can be extracted from the output characteristics according to Equation (1): $G = \frac{I_D}{V_D}$. The fitted straight lines from -40 V to -60 V in the G-function graphs of Figures S4 and S5 represent the values of slope (G, V_D) at different gate-source voltages (-60 V, -80 V and -100V), corresponding to the slopes in Equation (2).

$$R_C W = \left(\frac{1}{G} - \frac{1}{intercept + slope \times V_D}\right) \times W \qquad (2)$$

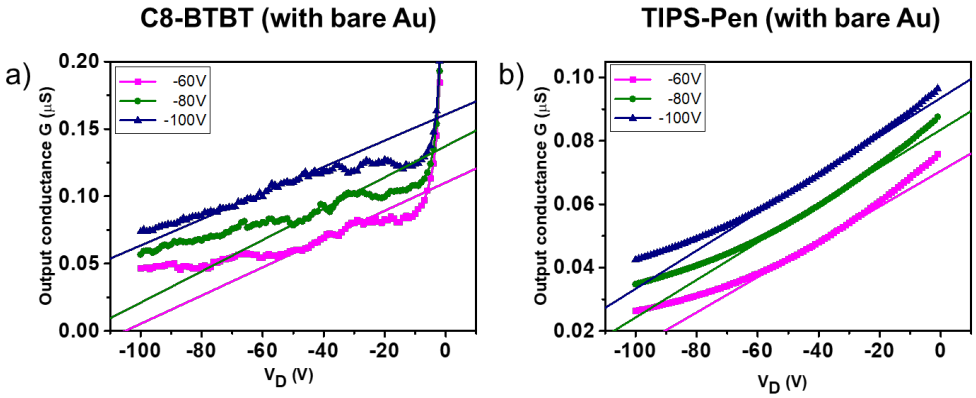

Figure S5. The graphs of output conductance G vs V_D at different gate-source voltages (-60 V, -80 V and -100V) for **a)** C8-BTBT **b)** TIPS-Pen based transistors with bare Au electrodes, respectively.

6. DFT calculations

1) Charge distribution in F-NHC molecules

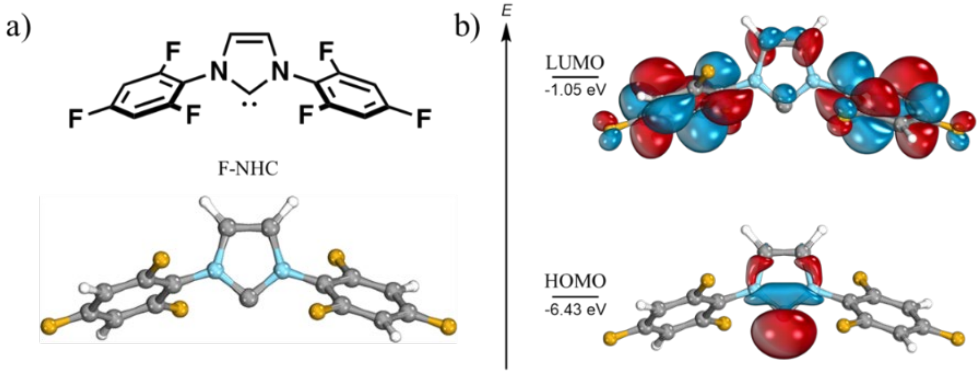

Figure S6. a) Chemical and geometry structure of Fluorine-substituted N-heterocyclic carbene (F-NHC). **b)** Charge distribution of the highest occupied molecular orbital (HOMO) and the lowest unoccupied molecular orbital (LUMO) in the structure of F-NHC calculated at the B3LYP D3/def2-QZVPP level of theory (isosurface density threshold = 80%).

Using different computational methodologies, significant differences within the absolute energy values of HOMO and LUMO are obtained. A consistent trend can only be observed when comparing carbene F-NHC to IPr, which was computed as a reference: In particular the most established hybrid functionals show a decrease in HOMO energy by ~0.4 eV moving from IPr to F-NHC, whereas the LUMO energy is decreased by ~0.5 eV.

Table S1. HOMO and LUMO energy level values of isolated F-NHC and IPr calculated using different methods.

Carbenes	IPr		F-NHC	
	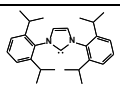		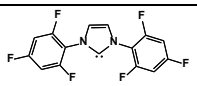	
Method	E_{HOMO}	E_{LUMO}	E_{HOMO}	E_{LUMO}
Literature[6] *(B3LYP / def2-TZVPP)*	*–5.97 eV*	*–0.46 eV*		
B3LYP D3 / def2-QZVPP	–6.05 eV	–0.48 eV	–6.43 eV	–1.05 eV
CAM-B3LYP D3 / def2-QZVPP	–7.73 eV	+0.75 eV	–8.15 eV	–0.21 eV
M06-2X / def2-QZVPP	–7.64 eV	+0.40 eV	–8.06 eV	–0.06 eV
PBE D3 / def2-QZVPP	–4.89 eV	–1.22 eV	–5.20 eV	–1.71 eV
TPSS D3 / def2-QZVPP	–5.01 eV	–1.03 eV	–5.34 eV	–1.56 eV
PBE0 D3 / def2-QZVPP	–6.29 eV	–0.30 eV	–6.67 eV	–0.84 eV
ωB97X-D3 / def2-QZVPP	–8.56 eV	+1.60 eV	–8.94 eV	+1.11 eV

Computational details for HOMO and LUMO energy levels: all computations were carried out using the ORCA 4.1.1 software suite.[7,8] Carbene geometry was optimized using the B3LYP functional[9] combined with Grimme's D3 dispersion correction[10,11] in the def2-TZVPP basis set.[12] The resulting geometry was confirmed to represent a local minimum by the absence of negative eigenvalues of the Hessian, as confirmed by a harmonic frequency calculation at the same level of theory. Frontier molecular orbital (FMO) energies were then computed using the def2-QZVPP basis set[12] using different density functional theory methods: One GGA functional (PBE[13]), two hybrid functionals (B3LYP,[9] PBE0[14]), a *meta*-GGA functional (TPSS[15]), a *meta*-GGA hybrid functional (M06-2X[16]), and two range-separated hybrid functionals (CAM-B3LYP,[17] ωB97X[18]). As a reference, similar computations were carried out for IPr.

2) Charge transfer

$$\Delta\rho = \rho_{Au+NHC} - \rho_{Au} - \rho_{NHC} \qquad (3)$$

The charge density difference is calculated by subtracting the charge densities of only the molecule ρ_{NHC} and only the Au atoms ρ_{Au} from the charge density of the full system $\rho_{\mathrm{Au+NHC}}$. The geometries of the single components were not relaxed for this purpose, instead the atoms of the respective counterpart were replaced by ghost atoms to avoid errors due to the change of basis set. The net charge transfer q is calculated by integration over $\Delta\rho(z)$:

$$q = \int_0^{zb} \Delta\rho(z)\, dz \qquad (4)$$

where the boundary z_b up to which the integral is evaluated is chosen such that q is maximal. It should be noted, that the plane at z_b might not be a good intersection between molecule and surface due to the bending of the molecule and the extraction of one surface atom. The intersection for F-NHC is indicated in Figure 5b.

The net charge transfer q for F-NHC is 0.40 $|e|$.

The total charge transfer can also be calculated by evaluating partial atomic charges.[19-21] The sum over all partial charges of the molecule's atoms gives the charge transfer into the surface. The calculations were performed using Löwdin,[19] Hirshfeld,[20] and Mulliken[21] partial charges. Detailed results are presented in Table S2.

Computational details for functionalized gold surface: all calculations of the functionalized gold surface employed the Cp2k 6.1 program package[22] which employs a mixed Gaussian and plane wave basis set. A DZVP basis set[23] (DZVP-SR for Au) was chosen and a planewave cutoff of 400 Ry. The PBE density functional[13] and normconserving Goedecker-Teter-Hutter pseudopotentials[24-26] were used. 700 additional orbitals were calculated together with Fermi-Dirac smearing with an electronic temperature of 300 K. Van der Waals interactions were included by employing D3 dispersion correction with Becke-Johnson damping (BJ).[10,11] The SCF convergence criterion was set to 10^{-6} a.u. The Au(111) surface was modelled using a slab of five atomic layers with a vacuum region of at least 32 Å between periodically repeated surfaces. The electrostatic potential is corrected for possible dipole interactions between the slabs.[27] An 8×8 Au(111) super cell was chosen, which corresponds to a coverage of 2.17×10^{13} molecules/cm^2 if one molecule is within the cell. The atomic positions of the upper two gold layers and the molecule were relaxed, until forces were smaller than 4.5×10^{-4} a.u. All properties were calculated at the Γ-point. This approximation can result in errors in adsorption energies of up to 0.1 eV.[28] The PBE+D3 optimized lattice constant of gold is in good agreement with the experimental value,[29] therefore an Au(111) lattice constant of 2.8835 Å is chosen.

Table S2. The summary of charge transfer for F-NHC on gold surface (coverage of 2×10^{13} molecules cm^{-2}) calculated using DFT.

		F-NHC/Au
Charge transfer (*e*)	*q* from density difference[a)]	0.40
	Mulliken	0.6
	Hirshfeld	2.0
	Löwdin	2.2

a) Calculated using (3).

7. References

1. M. S. S. Jamil, S. Alkaabi and A. K. Brisdon, *Dalton. Trans.,* 2019, **48**, 9317-9327.
2. C. M. Crudden, J. H. Horton, I. I. Ebralidze, O. V. Zenkina, A. B. McLean, B. Drevniok, Z. She, H.-B. Kraatz, N. J. Mosey, T. Seki, E. C. Keske, J. D. Leake, A. RousinaWebb and G. Wu, *Nat. Chem.,* 2014, **6**, 409-414.
3. X. Bantreil and S. P. Nolan, *Nat. Protoc.,* 2011, **6**, 69-77.
4. A. Lv, M. Freitag, K. M. Chepiga, A. H. Schafer, F. Glorius and L. Chi, *Angew. Chem. Int. Ed.,* 2018*,* **57***,* 4792–4796*; Angew. Chem.,* 2018*,***130***,* 4883-4887.
5. C. Liu, T. Minari, Y. Xu, B. Yang, H. Chen, Q. Ke, X. Liu, H. C. Hsiao, C. Lee and Y.Y. Noh, *Org. Electron.,* 2015, **27**, 253-258.
6. H. Song, H. Kim and E. Lee, *Angew. Chem. Int. Ed.,* 2018, **57**, 8603-8607; *Angew. Chem.,* 2018, **130**, 8739-8743.
7. F. Neese, *Wiley Interdiscip. Rev. Comput. Mol. Sci.,* 2012, **2**, 73-78.
8. F. Neese, Software update: the ORCA program system, version 4.0, *Wiley Interdiscip. Rev. Comput. Mol. Sci.,* 2018, **8**, DOI 10.1002/wcms.1327.
9. P. J. Stephens, F. J. Devlin, C. F. Chabalowski and M. J. Frisch, *J. Phys. Chem.,* 1994, ***98***, 11623-11627.
10. S. Grimme, J. Antony, S. Ehrlich and H. Krieg, *J. Chem. Phys.,* 2010, **132**, 241722.
11. S. Grimme, S. Ehrlich and L. Goerigk, *J. Comput. Chem.,* 2011, **32**, 1456-1465.
12. F. Weigend and R. Ahlrichs, *Phys. Chem. Chem. Phys.,* 2005, **7**, 3297-3305.
13. J. P. Perdew, K. Burke and M. Ernzerhof, *Phys. Rev. Lett.,* 1996, **77**, 3865-3868.
14. C. Adamo and V. Barone, *J. Chem. Phys.,* 1999, **110**, 6158-6170.
15. J. Tao, J. P. Perdew, V. N. Staroverov and G. E. Scuseria, *Phys. Rev. Lett.,* 2003, **91**, 146401.
16. Y. Zhao and D. G. Truhlar, *Theor. Chem. Acc.,* 2008, **120**, 215-241.
17. T. Yanai, D. P. Tew and N. C. Handy, *Chem. Phys. Lett.,* 2004, **393**, 51-57.

18. Y. S. Lin, G. D. Li, S. P. Mao and J. D. Chai, *J. Chem. Theory Comput.,* 2013, **9**, 263-272.
19. P.-O. Löwdin, *Adv. Quantum Chem.,* 1970, **5***,* 185-199.
20. F. L. Hirshfeld, *Theor. Chem. Acc.,* 1977, **44**, 129–138.
21. R. S. Mulliken, *J. Chem. Phys*., 1955, **23**, 1841-1846.
22. A. CP2k, "General program to perform molecular dynamics simulations". CP2k developers group under the terms of the GNU General Public License.
23. J. VandeVondele and J. Hutter, *J. Chem. Phys.,* 2007, **127**, 114105.
24. S. Goedecker, M. Teter and J. Hutter, *Phys. Rev. B,* 1996, **54**, 1703-1710.
25. C. Hartwigsen, S. Goedecker and J. Hutter, *Phys. Rev. B,* 1998, **58**, 3641-3662.
26. M. Krack, *Theor. Chem. Acc.,* 2005, **114**, 145-152.
27. L. Bengtsson, *Phys. Rev. B*, 1999, **59**, 12301.
28. M. C. Börner and J. Neugebauer, *Phys. Chem. Chem. Phys.,* 2019, **21**, 24926–24934.
29. W. Reckien, F. Janetzko, M. F. Peintinger and T. Bredow, *J. Comput. Chem.,* 2012, **33**, 2023-2031.